Towards Novel Herbicide Modes of Action by Inhibiting Lysine Biosynthesis in Plants

Tatiana P. Soares da Costa[1#*], Cody J. Hall[1#], Santosh Panjikar[2,3], Jessica A. Wyllie[1], Rebecca M. Christoff[4], Saadi Bayat[4], Mark D. Hulett[1], Belinda M. Abbott[4], Anthony R. Gendall[5,6], Matthew A. Perugini[1*]

[1] Department of Biochemistry and Genetics, La Trobe Institute for Molecular Science, La Trobe University, Bundoora, VIC 3086, Australia.

[2] Australian Synchrotron, ANSTO, 800 Blackburn Road, Clayton, VIC 3168, Australia.

[3] Department of Molecular Biology and Biochemistry, Monash University, Melbourne, VIC 3800, Australia.

[4] Department of Chemistry and Physics, La Trobe Institute for Molecular Science, La Trobe University, Bundoora, VIC 3086, Australia.

[5] Department of Animal, Plant and Soil Sciences, AgriBio, La Trobe University, Bundoora, VIC 3086, Australia.

[6] Australian Research Council Research Hub for Medicinal Agriculture.

[#] T.P.S.C. and C.J.H. are joint first authors

[*] Correspondence:

T. P. Soares da Costa, Department of Biochemistry and Genetics, La Trobe University, Bundoora, VIC 3086, Australia

Tel. (+61) 3 9479 2227

E-mail: T.SoaresdaCosta@latrobe.edu.au

M. A. Perugini, Department of Biochemistry and Genetics, La Trobe University, Bundoora, VIC 3086, Australia

Tel. (+61) 3 9479 6570

E-mail: M.Perugini@latrobe.edu.au

Abstract

Weeds are becoming increasingly resistant to our current herbicides, posing a significant threat to agricultural production. Therefore, new herbicides are urgently needed. In this study, we exploited a novel herbicide target, dihydrodipicolinate synthase (DHDPS), which catalyses the first and rate-limiting step in lysine biosynthesis. Using a high throughput chemical screen, we identified the first class of plant DHDPS inhibitors that have micromolar potency against *Arabidopsis thaliana* DHDPS isoforms. Employing X-ray crystallography, we determined that this class of inhibitors binds to a novel and unexplored pocket within DHDPS, which is highly conserved across plant species. We also demonstrated that the inhibitors attenuated the germination and growth of *A. thaliana* seedlings and confirmed their pre-emergence herbicidal activity in soil-grown plants. These results provide proof-of-concept that lysine biosynthesis represents a promising target for the development of herbicides with a novel mode of action to tackle the global rise of herbicide resistant weeds.

Introduction

Our ability to provide food security for a growing world population is being increasingly challenged by the emergence and spread of herbicide resistant weeds. Resistance has now been observed to the most widely used classes of herbicides. This includes amino acid biosynthesis inhibitors such as chlorsulfuron, glufosinate and glyphosate, which target enzymes in the biosynthetic pathways leading to the production of branched-chain amino acids, glutamine and aromatic amino acids, respectively (Duke, 2012; Hall et al., 2020; Heap, 2021, 2014; Vats, 2015). The impact of herbicide resistance is exacerbated by the lack of new herbicides entering the market in the past 30 years, especially those with new mechanisms of action (Duke, 2012). Nevertheless, the successful commercialisation of such herbicides provides proof-of-concept that targeting the biosynthesis of amino acids offers an excellent strategy for herbicide development (Hall et al., 2020). Amino acids are not only essential building blocks for protein biosynthesis, but they also play important roles in physiological processes that are critical for plant growth and development, such as carbon and nitrogen metabolism, in addition to serving as precursors to a wide range of secondary metabolites (Hildebrandt et al., 2015).

One amino acid biosynthesis pathway that remains largely unexplored for herbicide development is the diaminopimelate (DAP) pathway (Figure 1), which is responsible for the production of L-lysine (here after referred to as lysine) in plants and bacteria (Figure 1) (Hall and Soares da Costa, 2018). Animals, including humans, do not synthesise lysine, and therefore, must acquire it from dietary sources (Galili and Amir, 2013; Tomé and Bos, 2007). Consequently, specific chemical inhibition of the DAP pathway in plants is unlikely to result in cytotoxicity to animals and humans (Hutton et al., 2007). The DAP pathway commences with a condensation reaction between L-aspartate semialdehyde (ASA) and pyruvate to form (4*S*)-4-hydroxy-2,3,4,5-tetrahydro-(2*S*)-dipicolinic acid (HTPA), catalysed by HTPA synthase (EC 4.2.1.52), also known as dihydrodipicolinate synthase (DHDPS) (Griffin et al., 2012; Soares da Costa et al., 2017, 2015). HTPA is then reduced by dihydrodipicolinate reductase (DHDPR, EC 1.3.1.26) in the presence of NAD(P)H to produce 2,3,4,5-tetrahydrodipicolinate (THDP) (Christensen et al., 2016). In plants, THDP undergoes an amino-transfer by diaminopimelate aminotransferase (DAPAT, EC 2.6.1.83) to form L,L-DAP, which is converted to *meso*-DAP by diaminopimelate epimerase (DAPEpi, EC 5.1.1.7) (Hudson et al., 2005; McCoy et al., 2006). Lastly, *meso*-DAP is irreversibly decarboxylated by diaminopimelate decarboxylase (DAPDC, EC 4.1.1.20) to produce lysine (Peverelli and

Perugini, 2015). Lysine regulates flux through the pathway by binding allosterically to DHDPS and inhibiting the enzyme. Thus, DHDPS catalyses the rate-limiting step of the DAP pathway (Geng et al., 2013; Soares da Costa et al., 2016).

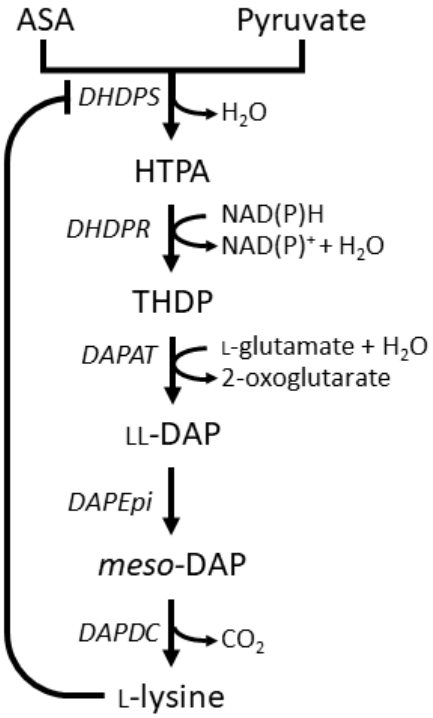

Figure 1: Lysine biosynthesis in plants. Plants utilise the diaminopimelate (DAP) pathway, a branch of the aspartate-derived super-pathway, to synthesise L-lysine. Firstly, L-aspartate semialdehyde (ASA) and pyruvate are converted to (4*S*)-4-hydroxy-2,3,4,5-tetrahydro-(2*S*)-dipicolinic acid (HTPA) in a condensation reaction catalysed by dihydrodipicolinate synthase (DHDPS). Dihydrodipicolinate reductase (DHDPR) then catalyses an NAD(P)H-dependent reduction of HTPA to produce 2,3,4,5-tetrahydrodipicolinte (THDP). THDP subsequently undergoes an amino-transfer reaction with L-glutamate, catalysed by diaminopimelate aminotransferase (DAPAT), to yield L,L-DAP. L,L-DAP is converted to *meso*-DAP by diaminopimelate epimerase (DAPEpi) and lastly, *meso*-DAP is decarboxylated by diaminopimelate decarboxylase (DAPDC) to yield L-lysine, which imparts a negative feedback loop on DHDPS.

Due to the central role of DHDPS in lysine production in plants, this enzyme has been proposed as a potential target for the development of herbicides (Griffin et al., 2012; Soares da Costa et al., 2017). Indeed, the lysine analogue *S*-(2-aminoethyl)-L-cysteine, has been shown to halt rooting of potato tuber discs at mid-micromolar concentrations (Perl et al., 1993; Ghislain et

al., 1995). However, given its poor *in vitro* potency against plant DHDPS, it is believed that this analogue inhibits plant growth by competing with lysine for incorporation into proteins rather than inhibition of the DHDPS enzyme (Ghislain et al., 1995; Perl et al., 1993). Plants typically have two annotated DHDPS-encoding genes (*DHDPS*) (Supplementary Figure 1) (Craciun et al., 2000; Sarrobert et al., 2000; Vauterin and Jacobs, 1994). In *Arabidopsis thaliana*, these genes are *At3G60880* (*DHDPS1*) and *At2G45440* (*DHDPS2*), which encode chloroplast-targeted AtDHDPS1 and AtDHDPS2, respectively (Jones-Held et al., 2012). Double knockouts of *DHDPS1* and *DHDPS2* result in non-viable embryos even after exogenous supplementation with lysine, indicating that DHDPS activity is essential (Jones-Held et al., 2012). AtDHDPS enzymes exist as homotetramers (Figure 2A), with the active site located within the $(\beta/\alpha)_8$-barrel (Figure 2B) and the allosteric cleft in the tight-dimer interface located in the interior of the structure (Figure 2C) (Griffin et al., 2012; Hall et al., 2021).

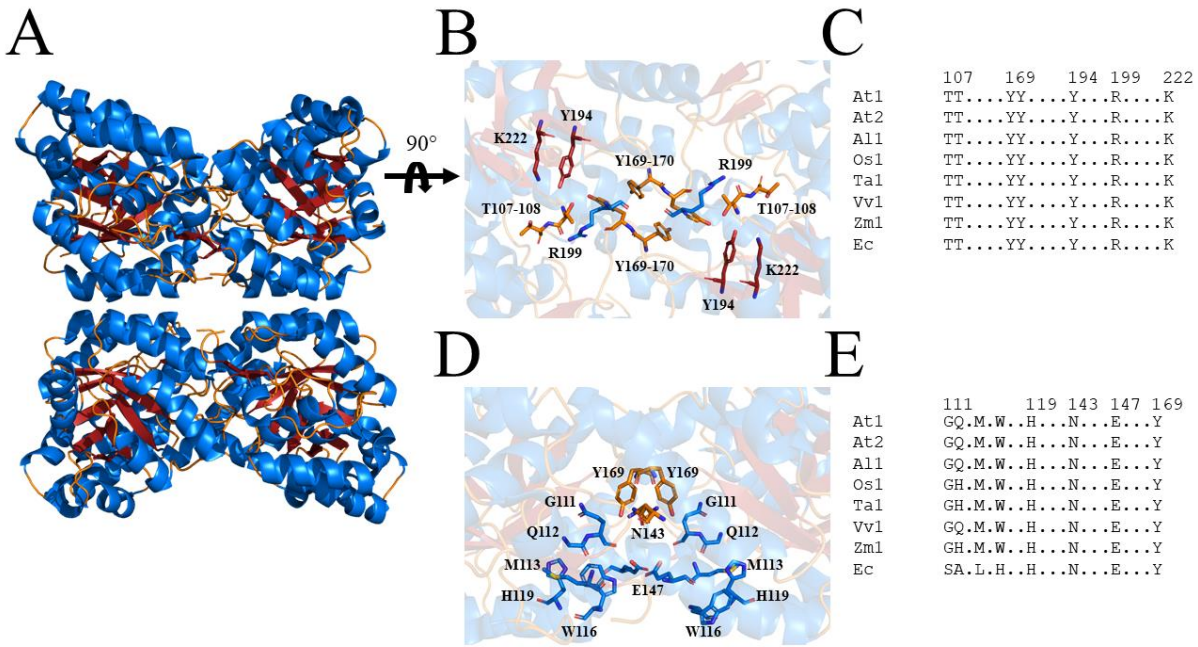

Figure 2: Structure and sequence conservation of plant DHDPS enzymes. (A) Cartoon structure of *Arabidopsis thaliana* (At) DHDPS1 (PDB: 6VVI) in the unliganded form illustrating the 'back-to-back' homotetramer conformation. (B) Cartoon structure of AtDHDPS1, with residues critical for catalysis shown as sticks. (C) Multiple sequence alignment of residues important for catalysis. (D) Cartoon structure of AtDHDPS1, with residues important for lysine binding and allosteric regulation shown as sticks. Residues are coloured by nitrogen (blue), oxygen (red) and sulfur (yellow). Images were generated using *PyMOL* v 2.2 (Schrödinger). (E) Multiple sequence alignment of residues involved in allosteric

lysine binding. Sequences are AtDHDPS1 (At1; UNIPROT ID: Q9LZX6), AtDHDPS2 (At2; UNIPROT ID: Q9FVC8), *Arabidopsis lyrata* DHDPS1 (Al1; UNIPROT ID: D7LRV3) *Oryza sativa* DHDPS1 (Os1; UNIPROT ID: A0A0K0K9A6), *Triticum aestivum* DHDPS1 (Ta1; UNIPROT ID: P24846), *Vitis vinifera* DHDPS1 (Vv1; UNIPROT ID: A0A438E022), *Zea mays* DHDPS1 (Zm1; UNIPROT ID: P26259) and *Escherichia coli* (Ec) DHDPS (UNIPROT ID: P0A6L2). Residues are numbered according to AtDHDPS1 with dots (.) representing interspacing residues. Sequences were aligned in *BioEdit* (v 7.2.5) (Hall, 1999) using the *ClustalW* algorithm (Thompson et al., 1994).

In this study, we describe the first class of plant DHDPS inhibitors. We show that these compounds display micromolar potency *in vitro* and *in planta* against *A. thaliana* using a combination of enzyme kinetics, seedling and soil assays, whilst exhibiting no cytotoxic effects in bacterial or human cell lines at equivalent concentrations. Furthermore, we employ X-ray crystallography to show these compounds target a previously unexplored binding site within DHDPS, which is highly conserved amongst plant species. Thus, this study provides proof-of-concept that lysine biosynthesis represents a promising pathway to target for the development of herbicides with a new mode of action and highlights a novel DHDPS binding pocket to assist in the discovery of herbicide candidates.

Results

High throughput chemical screen for inhibitor discovery

A high throughput screen of a library of 87,648 compounds was conducted against recombinant DHDPS enzyme by the Walter and Eliza Hall Institute High Throughput Chemical Screening Facility (Melbourne, Australia). The *o*-aminobenzaldehyde (*o*-ABA) colourimetric assay was used to estimate DHDPS activity via the formation of a purple chromophore that can be measured at 520-540 nm (Yugari and Gilvarg, 1965). Using a cut-off equal to the mean ± 3× standard deviation for classification as a hit compound, 435 compounds out of 87,648 were identified as hits at 20 mM (hit rate = 0.50%). The activity of these 435 compounds was confirmed at the same concentration as the primary screen, resulting in 38 compounds demonstrating >40% inhibition of the DHDPS enzymatic reaction (confirmation rate = 8.7%). A counter screen was employed to exclude false-positive compounds i.e., compounds that interacted with *o*-ABA detection or absorbance quantification. The compounds that displayed confirmed DHDPS inhibition were subsequently progressed to full dose response titration

assays using recombinant DHDPS. One promising compound from the screen was (*Z*)-2-(5-(4-fluorobenzylidene)-2,4-dioxothiazolidin-3-yl)acetic acid (FBDTA). The characterisation of two thiazolidinedione analogues containing methoxy substituents, MBDTA-1 and MBDTA-2, will be discussed here (Figure 3).

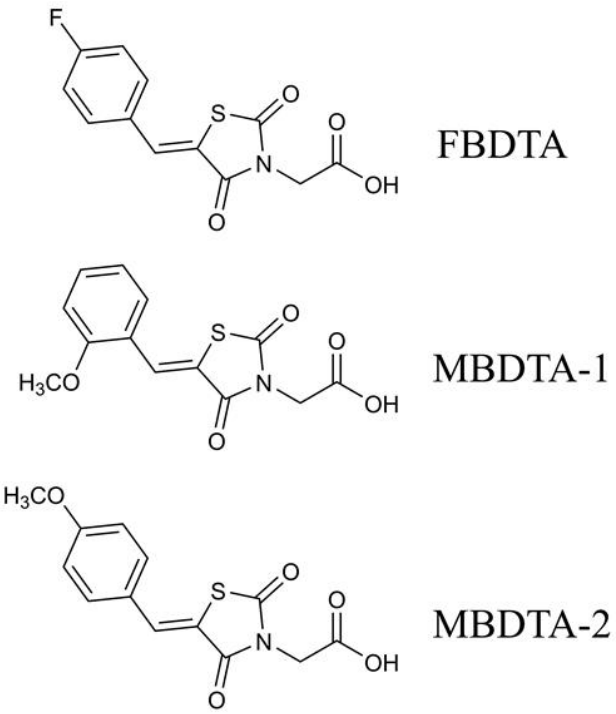

Figure 3: Structure of DHDPS inhibitors. Chemical structures of the hit compound, (*Z*)-2-(5-(4-fluorobenzylidene)-2,4-dioxothiazolidin-3-yl)acetic acid (FBDTA), and two analogues, (*Z*)-2-(5-(2-methoxybenzylidene)-2,4-dioxothiazolidin-3-yl)acetic acid (MBDTA-1) and (*Z*)-2-(5-(4-methoxybenzylidene)-2,4-dioxothiazolidin-3-yl)acetic acid (MBDTA-2). Image was generated using *ChemDraw* v 18.1 (PerkinElmer).

Efficacy of inhibitors on recombinant DHDPS

The inhibitory activity of MBDTA-1 and MBDTA-2 against both recombinant *A. thaliana* DHDPS proteins was quantitated using a DHDPS-DHDPR coupled assay (Atkinson et al., 2013). This was achieved by titrating different concentrations of each compound with substrates fixed at previously determined Michaelis-Menten constant values (Griffin et al., 2012; Hall et al., 2021). The IC_{50} values of MBDTA-1 and MBDTA-2 against AtDHDPS1 were determined to be 126 ± 6.50 µM and 63.3 ± 1.80 µM, respectively (Figure 4A). Similarly, the dose response curves for AtDHDPS2 yielded IC_{50} values of 116 ± 5.20 µM and 64.0 ± 1.00 µM for MBDTA-1 and MBDTA-2, respectively (Figure 4B). As these compounds represent a

novel class of inhibitors of plant DHDPS, we set out to assess the mechanism of inhibition by examining the binding of MBDTA-2 to DHDPS using X-ray crystallography.

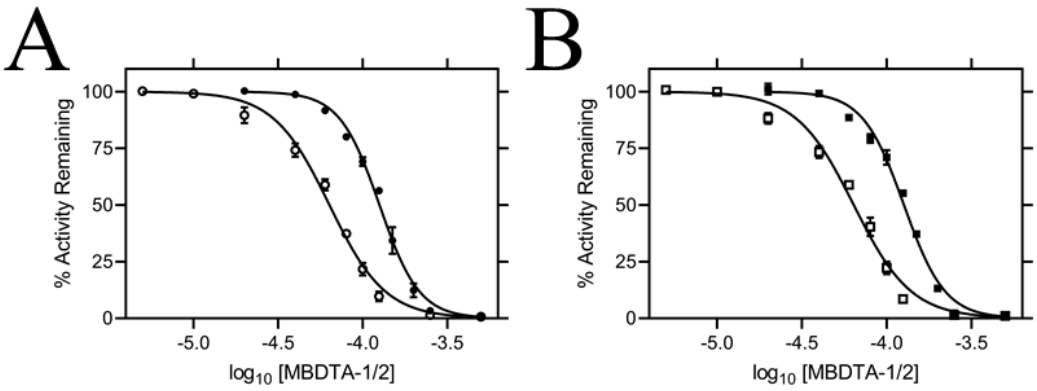

Figure 4: *In vitro* potency of DHDPS inhibitors. Dose responses of MBDTA-1 (● or ■) and MBDTA-2 (○ or □) against recombinant (A) AtDHDPS1 and (B) AtDHDPS2. Initial enzyme rates were normalised against a vehicle control (1% (v/v) DMSO). Normalised data (% activity remaining) is plotted as a function of $\log_{10}$[inhibitor] and fitted to a nonlinear regression model (solid line) ($R^2 = 0.99$). Data represents mean ± S.E.M. ($N = 3$).

Figure 4 – Source Data 1: *In vitro* dose response kinetic data.

Molecular basis for inhibitor binding

To probe the molecular determinants for inhibition, recombinant AtDHDPS1 was co-crystallised with MBDTA-2 using the same crystallisation conditions as for the apo enzyme with the addition of inhibitor (Hall et al., 2021). Diffraction data were obtained at a maximal resolution of 2.29 Å, phases solved by molecular replacement and repeating rounds of model building and refinement were performed that allowed us to generate an atomic inhibitor-bound model (Figure 5A, Table 1). We initially found several MBDTA-2 molecules at the crystal contact formed between protein molecules at chains B and D. Specifically, two parallel MBDTA-2 molecules were found bound to H187 (of the symmetry mate) and F210 with complete occupancy. However, given that these molecules were found solely at the crystal interface and were absent in chains A and C, they were assumed to be a result of non-specific binding.

Closer inspection of the crystal structure revealed the presence of four MBDTA-2 molecules bound at the center of the homotetrameric protein (Figure 5A), in antiparallel pairs with each

molecule, which were stabilised by interactions across three of the monomers (Figure 5B). Interestingly, this pocket, albeit distinct to the lysine binding site, shares two residues with it, namely W116 and E147 (Figure 2C). Specifically, the methoxy group of MBDTA-2 interacts with W116, E147 and H150 from chain B, while the carboxyl tail interacts with S115 from chain A as well as H150 and Q154 from chain C (Figure 5C). Additionally, we observed that upon binding, MBDTA-2 forces D117 to adopt a different rotamer conformation, which in turn, results in W116 assuming a different conformation. It must be noted that the four MBDTA-2 molecules were present with 50% occupancy. Consequently, each of the two moving residues, D117 and W116, adopt two distinct rotamer conformations, one of the apo- and one of the ligand-bound states of AtDHDPS1. Given that no major rotamer changes or movement of catalytically important residues were noted, the exact mechanism of inhibition remains elusive. Nevertheless, this indicates the presence of a novel DHDPS allosteric pocket that has not been previously exploited for inhibitor discovery. Moreover, an alignment of the primary structure of several DHDPS enzymes from plant species indicates that the residues involved in MBDTA-2 binding are highly conserved across both monocotyledons and dicotyledons (Figure 5D), and therefore should allow for broad spectrum inhibition.

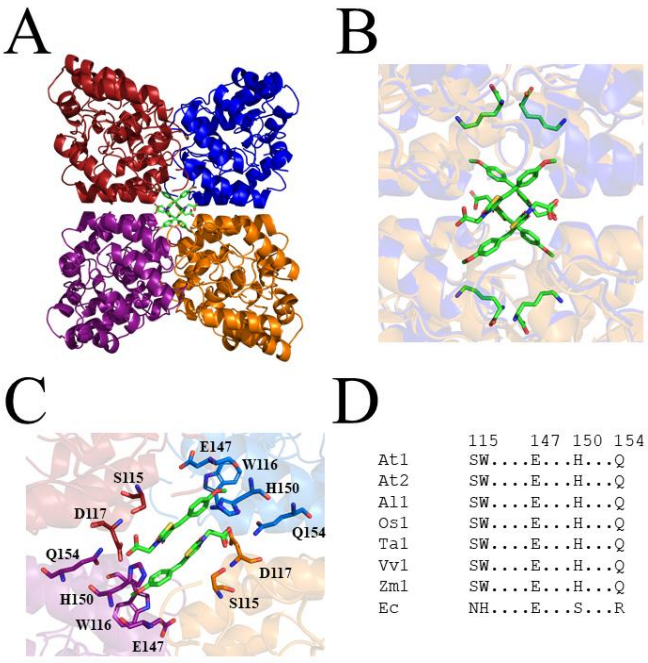

Figure 5: Crystal structure of AtDHDPS1 bound to MBDTA-2. (A) Cartoon view of overall AtDHDPS1 quaternary (tetrameric) structure, illustrating the binding sites for MBDTA-2 at the center of the tetramer. (B) Overlay of the lysine-bound (PDB: 6VVH) and MBDTA-2 bound structures. (C) Close-up of inhibitor binding pocket, with interacting residues shown as

sticks. Lysine and MBDTA-2 are shown as green sticks and coloured by nitrogen (blue), oxygen (red) and sulfur (yellow). Images were generated using *PyMOL* v 2.2 (Schrödinger). (D) Sequence alignment of residues involved in MBDTA-2 binding from *A. thaliana* DHDPS1 (At1; UNIPROT ID: Q9LZX6), *A. thaliana* DHDPS2 (At2; UNIPROT ID: Q9FVC8), *A. lyrata* DHDPS1 (Al1; UNIPROT ID: D7LRV3), *O. sativa* DHDPS1 (Os1; UNIPROT ID: A0A0K0K9A6), *T. aestivum* DHDPS1 (Ta1; UNIPROT ID: P24846), *V. vinifera* DHDPS1 (Vv1; UNIPROT ID: A0A438E022), *Z. mays* DHDPS1 (Zm1; UNIPROT ID: P26259), and *E. coli* (Ec) DHDPS (UNIPROT ID: P0A6L2). Residues are numbered according to *A. thaliana* DHDPS1 with dots (.) representing interspacing residues. Sequences were aligned in *BioEdit* (v 7.2.5) using the *ClustalW* algorithm.

Table 1: Summary of MBDTA-2 bound AtDHDPS1 crystallographic data collection, processing and refinement statistics.

Data collection	AtDHDPS1 + MBDTA-2
Space group	$P4_12_12$
Unit cell parameters (Å)	94.47, 94.47, 181.41
Resolution (Å)	20-2.29 (2.43-2.29)
No. of observations	491320 (74297)
No. of unique reflections	37390 (5768)
Completeness (%)	99.4 (96.6)
Redundancy	13.1 (12.8)
R_{merge} (%)	9.9 (39.1)
R_{meas} (%)	10.0 (40.7)
$CC_{1/2}$	99.9 (97.8)
Average $I/\sigma(I)$	27.9 (7.9)
Refinement	
R (%)	18.3
R_{free} (%)	22.6
No. (%) of reflections in test set	1071
No. of protein molecules per asu	2
r.m.s.d bond length (Å)	0.007
r.m.s.d bond angle (°)	1.415
Average B-factors (Å^2) [a]	

Protein molecules	44.52
Ligand molecules	60.01
Water molecules	40.33
Ramachandran plot [b]	
Residues other than Gly and Pro in:	
Most favored regions (%)	98.0
Additionally allowed regions (%)	2.0
Disallowed regions (%)	0.0
PDB code	7MDS

Values in parentheses are for the highest-resolution shell.

[a] Calculated by *BAVERAGE* in CCP4 Suite (Winn et al., 2011).

[b] Calculated using *MolProbity* (Chen et al., 2010).

Specificity of DHDPS inhibitors

Following determination of the binding site, we examined the specificity of MBDTA-1 and MBDTA-2 to determine if any future applications would have off-target effects. Firstly, the cytotoxicity of the inhibitors was examined against the HepG2 and HEK293 cell lines using the 3-(4,5-dimethylthiazol-2-yl)-2,5-diphenyltetrazolium bromide (MTT) assay (Supplementary Figure 2A-B). At the highest concentration assessed (400 µM), treatment with the inhibitors did not affect the viability of either cell line relative to the vehicle control. Secondly, the effect of the inhibitors on several bacterial species commonly found in the human flora and soil microbiome was assessed by measuring their minimum inhibitory concentrations. No inhibition of bacterial growth was observed up to 128 $\mu g \cdot mL^{-1}$ (equivalent to ~400 µM) (Table 2), indicating that these DHDPS inhibitors have specificity directed towards plants.

Table 2: Minimum inhibitory concentration (MIC) values for MBDTA-1 and MBDTA-2 against several bacterial strains.

	MBDTA-1 MIC ($\mu g \cdot mL^{-1}$)	MBDTA-2 MIC ($\mu g \cdot mL^{-1}$)
Human Flora		
Enterococcus spp.	>128	>128
Staphylococcus aureus	>128	>128
Escherichia coli	>128	>128
Soil Bacteria		
Enterobacter ludwigii	>128	>128
Arthrobacter sp.	>128	>128
Enterobacter cancerogenus	>128	>128
Cedecea davisae	>128	>128
Rhodococcus erthropolis	>128	>128

Table 2 – Source Data 1: Antibacterial MIC data.

Herbicidal efficacy

Given the promising *in vitro* properties of the inhibitors, we determined their herbicidal efficacy against *A. thaliana*, initially using seedling agar assays. At high micromolar concentrations of both MBDTA-1 (Figure 6A) and MBDTA-2 (Figure 7A), growth was completely attenuated, and most seeds were unable to germinate. Upon quantitation of root lengths, we determined an IC_{50} of 98.1 ± 4.34 µM and 47.4 ± 0.450 µM for MBDTA-1 (Figure 6B) and MBDTA-2 (Figure 7B), respectively. Based on these results, we examined their pre-emergence effect on soil-grown *A. thaliana*. Specifically, compounds were dissolved in a solution containing a non-ionic organic surfactant (Agral) and seeds were treated immediately after sowing on soil. The vehicle control-treated plants (Figure 8A) were used as a benchmark to visually assess the effects of inhibitors. The growth of *A. thaliana* in the presence of MBDTA-1 (Figure 8B) or MBDTA-2 (Figure 8C) at 300 $mg \cdot L^{-1}$ was severely impeded as evidenced by the growth area relative to the DMSO control (Figure 8D), wherein few seeds

were able to germinate. This is consistent with the results observed at the highest concentrations of inhibitor on agar. Furthermore, the *A. thaliana* seeds capable of germinating in the presence of 300 $mg \cdot L^{-1}$ MBDTA-2 were halted at the cotyledon stage before the generation of true leaves. As such, our newly discovered MBDTA compounds represent the first DAP pathway inhibitors with soil efficacy against plants.

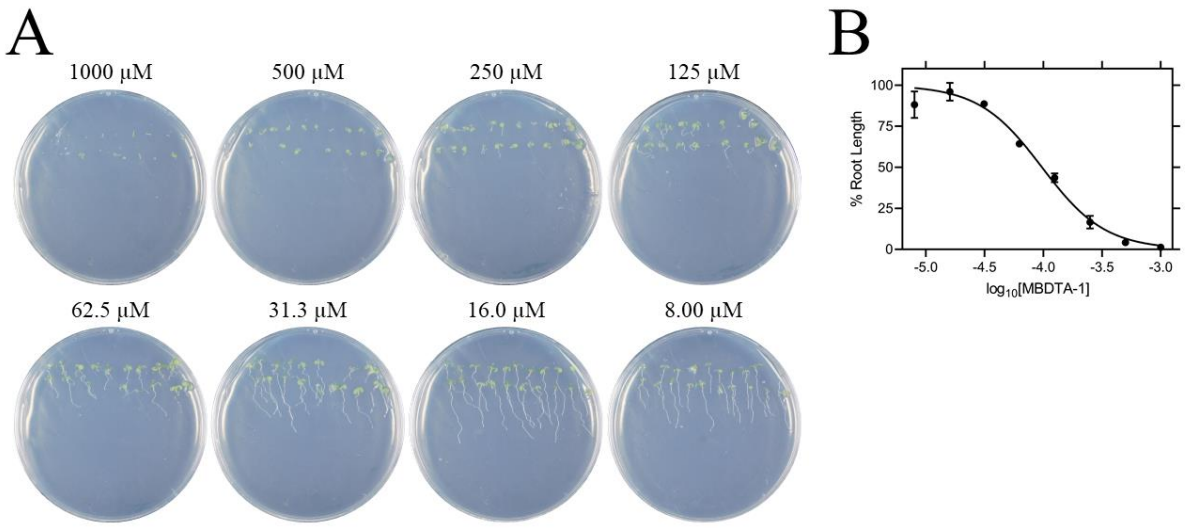

Figure 6: Effect of MBDTA-1 on agar-grown *A. thaliana*. (A) *A. thaliana* grown on Gamborg modified Murashige Skoog media treated with MBDTA-1 at varying concentrations after 7 days. (B) *A. thaliana* root lengths after treatment with increasing concentrations of MBDTA-1. Root lengths were determined using *ImageJ* v 1.53b and normalised against a vehicle control (1% (v/v) DMSO). Normalised data (●) (% root length) is plotted as a function of $\log_{10}$[inhibitor] and fitted to a nonlinear regression model (solid line) (R^2 = 0.99). Data represents mean ± S.E.M. (N = 3).

Figure 6 – Source Data 1: *In planta* MBDTA-1 dose response data.

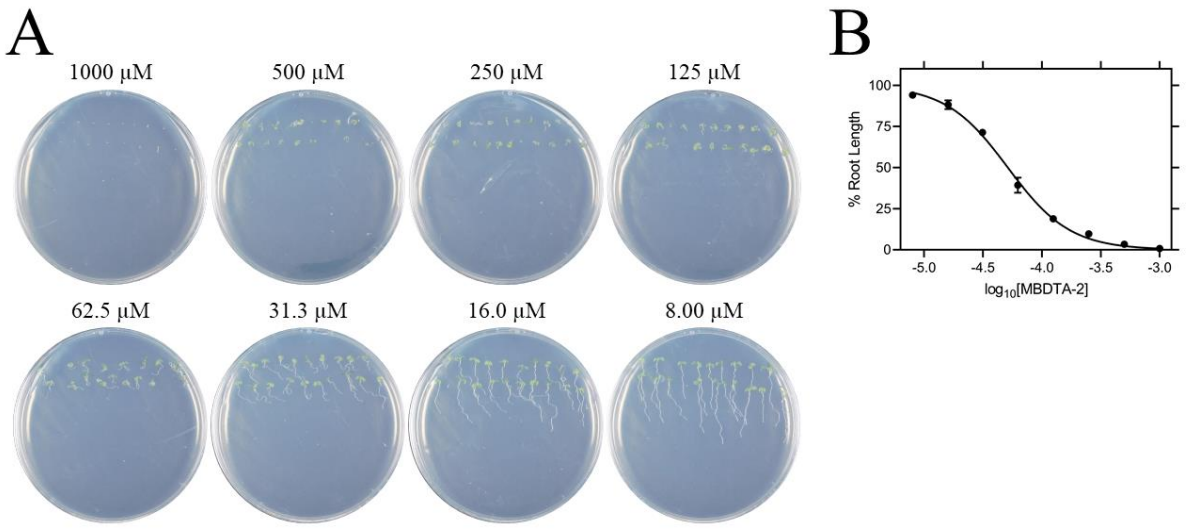

Figure 7: Effect of MBDTA-2 on agar-grown *A. thaliana*. (A) *A. thaliana* grown on Gamborg modified Murashige Skoog media treated with MBDTA-2 at varying concentrations after 7 days. (B) *A. thaliana* root lengths after treatment with increasing concentrations of MBDTA-2. Root lengths were determined using *ImageJ* v 1.53b and normalised against a vehicle control (1% (v/v) DMSO). Normalised data (●) (% root length) is plotted as a function of $\log_{10}$[inhibitor] and fitted to a nonlinear regression model (solid line) (R^2 = 0.99). Data represents mean ± S.E.M. (N = 3).

Figure 7 – Source Data 1: *In planta* MBDTA-2 dose response data.

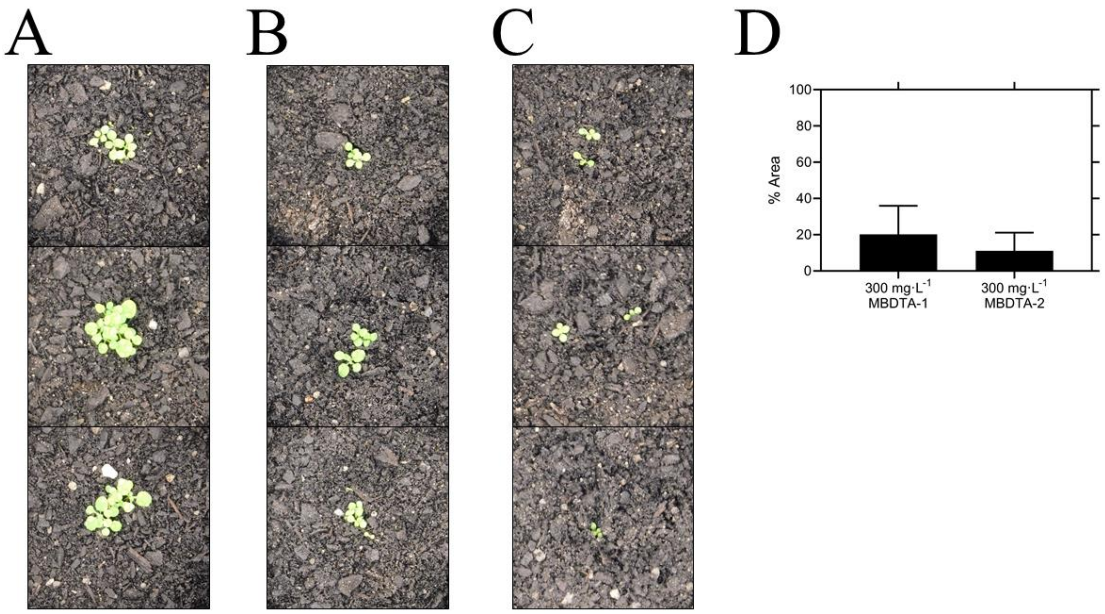

Figure 8: Pre-emergence efficacy of inhibitors on *A. thaliana* grown in soil. Treatments of (A) vehicle control (1% (v/v) DMSO), (B) 300 mg·L^{-1} MBDTA-1 and (C) 300 mg·L^{-1} MBDTA-2 given at day 0 (first day under controlled environment room conditions). A representative in triplicate of the biological replicates is shown vertically. (D) Leaf area of MBDTA-1/2 treated *A. thaliana*. Area was determined using *ImageJ* v 1.53b and normalised against a vehicle control (1% (v/v) DMSO). Data represents mean ± S.D. (n = 3).

Figure 8 – Source Data 1: *In planta* MBDTA-1/2 soil efficacy data.

Discussion

The lack of herbicides with novel modes of action entering the market in the past three decades has led to an over-reliance on our current agrichemicals, which has contributed to the rapid generation of resistance. Although the DAP pathway has gained attention as a way to increase the nutritional content of lysine in crops (Wang et al., 2017), it has remained an unexplored target for the development of herbicides until now. DHDPS catalyses the first step of the DAP pathway and is commonly duplicated in plant species, including *A. thaliana*. Both DHDPS proteins are localised to the chloroplast and share >85% of primary structure identity, with the majority of differences found at the N-terminus. Although DHDPS has been shown to be essential in *A. thaliana* (Jones-Held et al., 2012), there have been no published inhibitors of the plant enzymes, with much of the focus on inhibitors of bacterial DHDPS as possible new antibiotics.

Our study describes the discovery of the first plant DHDPS inhibitors, with two MBDTA analogues identified and characterised here. The mode of inhibition was shown to be via a novel binding pocket adjacent to the lysine binding site, which results in the allosteric inhibition of the enzyme. Lysine has recently been shown to differentially inhibit the AtDHDPS isoforms, with AtDHDPS1 being 10-fold more sensitive to the allosteric inhibitor (Hall et al., 2021). In this study, we demonstrate that the MBDTA compounds have similar inhibitory effects against both enzymes. This further supports our crystallography data that shows that MBDTA-2 binds in a pocket adjacent to the lysine allosteric site and is likely acting in a different way. However, the exact mechanism of inhibition, much like lysine-mediated allostery, remains elusive. Moreover, we found that this binding pocket is conserved across multiple plant species, including both monocots and dicots. Importantly, our compounds lacked off-target toxicity, whilst resulting in the inhibition of germination and growth of *A. thaliana* seedlings on solidified media and in soil. However, as expected, plant inhibition was more pronounced on media likely due to the stability, distribution and persistence of the compounds. Nevertheless, the assays performed on soil demonstrate their potential applicability as pre-emergence treatments. It would also be of interest to investigate the metabolic shifts in plants treated with inhibitors and determine if there is a toxic build-up of other amino acids such as threonine, which has been observed in *DHDPS* knockout experiments (Sarrobert et al., 2000). Indeed, a common trait of systemic herbicides is that their efficacy is often related to the cascading consequences of inhibiting a key reaction, rather than inhibition of the reaction itself (Hall et al., 2020).

Developing enzyme inhibitors into a commercial product is an arduous and costly process. Optimisation of phytotoxicity, water solubility, cell wall penetration, translocation, soil/water persistence and formulation must all be considered. The MBDTA compounds described here represent an attractive avenue to pursue and with the elucidation of a novel binding pocket within DHDPS, it may be possible to rationally improve their potency guided by the crystallography data. Alternatively, novel chemical scaffolds could be explored to target the DHDPS pocket identified. The inhibitors must be able to traverse the chloroplast membrane in order to reach the DHDPS target and be amenable to post-emergence application. It would also be of interest to study inhibitors with increased hydrophilicity and thus, potentially enhanced transport through the cell wall. Importantly, DHDPS inhibitors could also be used in conjunction with other herbicides as part of a combinatorial treatment to yield synergistic

responses and circumvent resistance mechanisms to tackle the global rise in herbicide resistant weeds.

Materials and Methods

High throughput chemical screen and analogue synthesis

A high throughput screen of a library of 87,648 compounds was conducted against recombinant DHDPS enzyme by the Walter and Eliza Hall Institute High Throughput Chemical Screening Facility (Melbourne, Australia). The *o*-ABA colourimetric assay employed assesses DHDPS activity via the formation of a purple chromophore that can be measured at 520-540 nm (Yugari and Gilvarg, 1965). The assay was miniaturised so it could be performed in 384-well plates. For the primary screen, reactions comprised 0.5 $mg \cdot mL^{-1}$ DHDPS, 0.5 mM sodium pyruvate and 0.5 mM ASA. Library compounds were added at final concentrations of 20 mM, with DMSO concentrations kept at 0.4% (v/v). After ASA addition, reactions were incubated at 25 °C for 15 mins, before a final concentration of 350 mM HCl was added to stop the reaction. *o*-ABA was subsequently added to a final concentration of 0.44 $mg \cdot mL^{-1}$, plates incubated at room temperature for 1 hr, and absorbance quantified at 540 nm. Vehicle (DMSO) was used as positive controls, and negative controls lacked ASA. For the secondary screen, 11-point dose response curves were generated using the same reactions as described above. A counter screen was conducted using the same set-up albeit without the inclusion library compounds before the addition of 350 mM HCl. Library compounds were then added after the reaction was stopped, followed by *o*-ABA to a final concentration of 0.44 $mg \cdot mL^{-1}$. The plates were subsequently incubated at room temperature for 1 hr, and absorbance quantified at 540 nm. Analogues were designed and synthesised using the methods described in previous and contemporary work (Perugini et al., 2018).

Expression and purification of *A. thaliana* DHDPS enzymes

Both DHDPS isoforms from *A. thaliana* were expressed and purified as previously described (Hall et al., 2021). Briefly, AtDHDPS isoforms were expressed in *Escherichia coli* BL21 (DE3) cells, with AtDHDPS2 requiring the GroEL/ES chaperone complex to facilitate correct folding. Purification was performed using immobilised metal affinity chromatography. Lastly, fusion tags were cleaved by human rhinovirus 3C or tobacco etch virus protease for AtDHDPS1 and AtDHDPS2, respectively, whilst simultaneously dialysing into storage buffer (20 mM Tris, 150 mM NaCl, 0.5 mM TCEP, pH 8.0).

Enzyme kinetics

DHDPS enzyme activity was determined using the DHDPS-DHDPR coupled assay as previously described by measuring the oxidation of NADPH (Atkinson et al., 2013; Hall et al., 2021). Assays were carried out in a Cary 4000 UV/Vis spectrophotometer at 30 °C with substrates fixed at the previously determined Michaelis-Menten constant values (Griffin et al., 2012; Hall et al., 2021). Inhibitor was titrated against AtDHDPS enzymes and reactions were incubated at 30 °C for 12 mins before initiation with ASA. Initial velocity data were normalised against a vehicle (DMSO) control and analysed using Equation 1 (log(inhibitor) vs. normalized response - variable slope, *GraphPad Prism* v 8.3). Dose responses were performed with 3 technical replicates for each concentration of compound. Dose responses were repeated with 3 biological replicates, each using a new stock of reagents.

Equation 1:

$$Y = 100/ (1 + 10^{((\mathrm{LogIC}_{50} - X) \times \mathrm{HillSlope})})$$

Where Y is the normalised rate, logIC_{50} is the logarithmic concentration of ligand resulting in 50% activity, X is the concentration of ligand, and Hill Slope is the steepness of the curve.

X-ray crystallography

AtDHDPS1 was co-crystallised as previously described in the presence of MBDTA-2 (Hall et al., 2021). Briefly, protein (8.5 $\mathrm{mg \cdot mL^{-1}}$) was incubated at 20 °C with MBDTA-2 at a final concentration of 1 mM (in 2% (v/v) DMSO) before being added in a 1:1 ratio to a reservoir solution containing 1.4 M $(NH_4)_2SO_4$, 0.1 M NaCl, 0.1 M HEPES (pH 7.5) and 1 mM MBDTA-2 (in 2% (v/v) DMSO). Plates were incubated at 20 °C. Crystals were briefly dipped in cryo-protectant (1.4 M $(NH_4)_2SO_4$, 0.1 M NaCl, 0.1 M HEPES (pH 7.5), 1 mM MBDTA-2 (in 2% (v/v) DMSO) and 20% (v/v) glycerol) and flash frozen in liquid nitrogen. Data were collected at the Australian Synchrotron using the MX2 beamline (Aragão et al., 2018). A total of 1800 diffraction images were collected with 0.1° oscillation using an EIGER 16M detector at a distance of 350 mm, with 20% beam attenuation for a total exposure time of 18 sec. X-ray data were integrated using *XDS* (Kabsch, 2010) and scaled with *AIMLESS* (Evans and Murshudov, 2013) before phases were determined by molecular replacement through *Auto-Rickshaw* (Panjikar et al., 2005) with AtDHDPS1 (PDB ID: 6VVI) used as a search model (Hall et al., 2021). Manual building was performed in *COOT* (Emsley et al., 2010) followed by refinement employing *REFMAC5* in the *CCP4i2* (v7.0) software suite (Emsley et al., 2010; Murshudov et al., 2011; Winn et al., 2011). SMILES string of the inhibitor (MBDTA-2) was

processed through *AceDRG* to generate the coordinate and cif file (Long et al., 2017). Validation was completed using *MolProbity* (Chen et al., 2010). The structure of MBDTA-2 bound to AtDHDPS1 is deposited in the Protein Data Bank as 7MDS.

Toxicity assays

The toxicity of inhibitors against human HepG2 and HEK293 cell lines was assessed using the MTT viability assay as previously described (Soares da Costa et al., 2012). In brief, the cells were suspended in Dulbecco-modified Eagle's medium containing 10% (v/v) fetal bovine serum and then seeded in 96-well tissue culture plates at 5,000 cells per well. After 24 hrs, cells were treated with 50 – 400 µM of MBDTA-1 or MBDTA-2, such that the DMSO concentration was consistent at 1% (v/v) in all wells. Alternatively, cells were treated with the cytotoxic defensin protein at 100 µM (Baxter et al., 2017). After treatment for 48 hrs, MTT cell proliferation reagent was added to each well and incubated for 3 hrs at 37 °C. The percentage viability remaining reported is relative to the vehicle control of 1% (v/v) DMSO. Assays were performed in 3 biological replicates, using a different batch of reagents and cells.

Antibacterial assays

The minimum inhibitory concentration (MIC) for MBDTA-1 and MBDTA-2 was determined against a panel of Gram-positive and Gram-negative bacteria using a broth microdilution method according to guidelines defined by the Clinical Laboratory Standards Institute (National Committee for Clinical Laboratory Standards, 2004, 2003). An inoculum of 1×10^5 colony forming units per mL was used and the testing conducted using tryptic soy broth in 96-well plates. Growth was assessed after incubation at 37 °C for 20 hrs by measuring the absorbance at 600 nm. The MIC value is defined as the lowest concentration of inhibitor where no bacterial growth is observed. Experiments were performed in 3 biological replicates, using a different stock of reagents and bacterial culture.

Seedling assays

Inhibitors were dissolved in 1× Gamborg modified/ Murashige Skoog (GM/MS) media to final concentrations of 8 – 1000 µM. Specifically, media were prepared with 0.8% (w/v) plant grade agar and 1% (w/v) sucrose before sterilisation (Lindsey et al., 2017). *A. thaliana* seeds were surface sterilised by soaking in 80% (v/v) ethanol for 5 mins, followed by a 15 min incubation in bleach solution containing 1% (v/v) active NaClO and rinsed in excess sterile water before placing onto agar-containing inhibitors (Boyes et al., 2001). *A. thaliana* seeds were stratified

at 4 °C for 72 hrs in the dark prior to relocation to a controlled environment room (CER), where seeds were grown at 22 ± 0.5 °C at 60 ± 10% humidity with light produced by cool white fluorescent lights at a rate of ~110 µmols·m^{-2}·s^{-1} over long-day conditions (16 hrs light: 8 hrs dark) (Boyes et al., 2001). Plates were positioned upright to allow roots to grow downwards and after 7 days, images were taken, and root length determined using *ImageJ* (v 1.53b) (Rasband, 2011). Outliers were identified using the 1.5 × interquartile range method (Tukey, 1977). Resulting data were analysed using Equation 1 (log(inhibitor) vs. normalized response - variable slope, *GraphPad Prism* v 8.3). No DMSO and vehicle (1% (v/v) DMSO) controls were also employed. Assays were carried out with 20 technical replicates (i.e. seeds) per experiment and were repeated in 3 biological replicates, with each biological replicate using a different stock of reagents and batch of seeds.

Soil assays

Inhibitors were prepared in DMSO and diluted to 300 mg·L^{-1} (1% (v/v) DMSO) in H_2O containing 0.01% (v/v) Agral (Syngenta, North Ryde, NSW, Australia). *A. thaliana* seeds were surface sterilised as above and resuspended in 0.1% (w/v) agar before stratification. Subsequently, ~30 seeds were sown into fine soil and treated with 1 mL of compound or vehicle control just prior to transfer to a CER and images taken after 7 days. Area analysis was performed using colour thresholding in *ImageJ* (v 1.53b) and normalised against the DMSO control (Corral et al., 2017; Rasband, 2011). Assays were carried out across 3 technical replicates (i.e., pots) using the same batch of reagents and seed stock.

Acknowledgements

T.P.S.C. would like to thank the National Health and Medical Research Council of Australia (APP1091976) and Australian Research Council (DE190100806) for fellowship and funding support, and M.A.P. and S.P. the Australian Research Council for funding support (DP150103313). A.R.G would like to thank the Australian Research Council Research Hub for Medicinal Agriculture (IH180100006) for support. C.J.H. is supported by La Trobe University Postgraduate Research scholarships. R.M.C. is a recipient of an Australian Government Research Training Program Scholarship and a LIMS Write-Up Award. This research was supported by the Defence Science Institute, an initiative of the State Government of Victoria, with a scholarship awarded to J.A.W, who is also the recipient of a Research Training Program scholarship. We thank Dr Grant Pearce (University of Canterbury, New Zealand) for supplying pET151/D-Topo harbouring the DHDPS2/*dapA2* gene and Professor Ashley Franks (La Trobe University, Australia) for supplying soil bacterial isolates. We acknowledge the use of the MX2 beamline at the Australian Synchrotron, part of ANSTO, and employed the Australian Cancer Research Foundation (ACRF) detector. We acknowledge the CSIRO Collaborative Crystallisation Centre (www.csiro/C3; Melbourne, Australia). We also thank the La Trobe University Comprehensive Proteomics Platform for providing infrastructure support.

Author contributions

T.P.S.C., C.J.H., S.P., B.M.A., A.R.G. and M.A.P. designed experiments; T.P.S.C., C.J.H., S.P., J.A.W., R.M.C. and S.B. performed experiments and analysed data; T.P.S.C. and C.J.H. wrote the manuscript; all authors provided revisions and edits.

Competing Interests

T.P.S.C., B.M.A. and M.A.P. are listed as inventors on a patent pertaining to inhibitors described in the manuscript. Patent Title: Heterocyclic inhibitors of lysine biosynthesis via the diaminopimelate pathway; International patent (PCT) No.: WO2018187845A1; Granted: 18/10/2018.

Supplementary Information

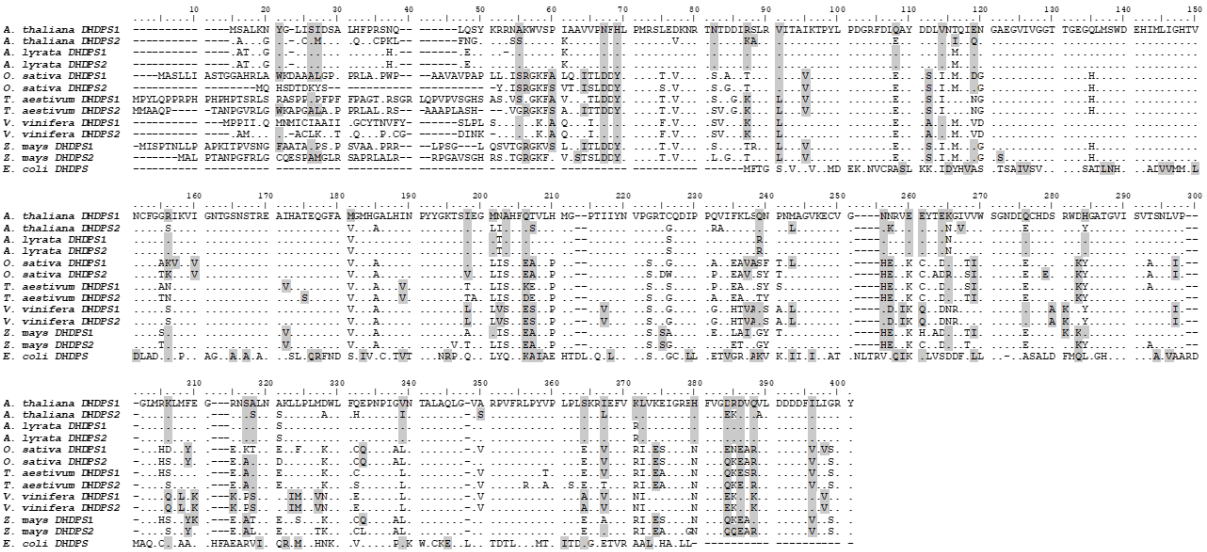

Supplementary Figure 1: Sequence alignment of plant DHDPS enzymes. *Arabidopsis thaliana* (At) DHDPS1 (UNIPROT ID: Q9LZX6), AtDHDPS2 (UNIPROT ID: Q9FVC8), *Arabidopsis lyrata* (Al) DHDPS1 (UNIPROT ID: D7LRV3), AlDHDPS2 (UNIPROT ID: D7LCJ3), *Oryza sativa* (Os) DHDPS1 (UNIPROT ID: A0A0K0K9A6), OsDHDPS2 (UNIPROT ID: Q9LWB9), *Triticum aestivum* (Ta) DHDPS1 (UNIPROT ID: P24846), TaDHDPS2 (UNIPROT ID: P24847), *Vitis vinifera* (Vv) DHDPS1 (UNIPROT ID: A0A438E022), Vv DHDPS2 (UNIPROT ID: D7U7T8), *Zea mays* (Zm) DHDPS1 (UNIPROT ID: P26259), ZmDHDPS2 (UNIPORT ID: B4FLW2), and *Escherichia coli* (Ec) DHDPS (UNIPROT ID: P0A6L2). Residues are numbered according to AtDHDPS1; identical residues are shown as dots (.), gaps are shown as dashes (-), and similar residues are highlighted in grey. Sequences were aligned in *BioEdit* (v 7.2.5) using the *ClustalW* algorithm.

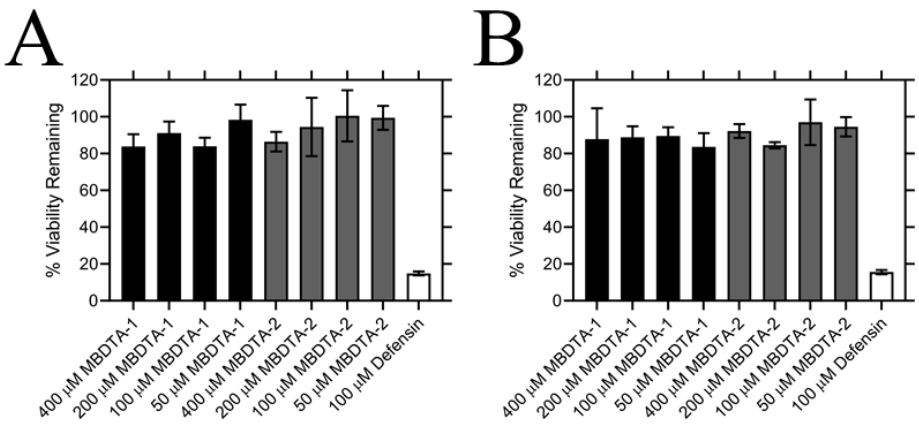

Supplementary Figure 2: Effect of compounds on the viability of human cell lines. Toxicity of MBDTA-1 (black) and MBDTA-2 (grey), compared to the positive control defensin (white), assessed against (A) HepG2 and (B) HEK293 human cell lines using the MTT assay. Data were normalised against a vehicle control (1% (v/v) DMSO) and plotted against inhibitor concentration. Data represents mean ± S.E.M. (N = 3).

Figure S2 – Source Data 1: MBDTA-1/2 mammalian cell toxicity data.

References

Aragão D, Aishima J, Cherukuvada H, Clarken R, Clift M, Cowieson NP, Ericsson DJ, Gee CL, Macedo S, Mudie N, Panjikar S, Price JR, Riboldi-Tunnicliffe A, Rostan R, Williamson R, Caradoc-Davies TT. 2018. MX2: a high-flux undulator microfocus beamline serving both the chemical and macromolecular crystallography communities at the Australian Synchrotron. *J Synchrotron Radiat* **25**:885–891. doi:10.1107/S1600577518003120

Atkinson SC, Dogovski C, Downton MT, Czabotar PE, Dobson RCJ, Gerrard JA, Wagner J, Perugini MA. 2013. Structural, kinetic and computational investigation of *Vitis vinifera* DHDPS reveals new insight into the mechanism of lysine-mediated allosteric inhibition. *Plant Mol Biol* **81**:431–446. doi:10.1007/s11103-013-0014-7

Baxter AA, Poon IK, Hulett MD. 2017. The plant defensin NaD1 induces tumor cell death via a non-apoptotic, membranolytic process. *Cell Death Discov* **3**:16102. doi:10.1038/cddiscovery.2016.102

Boyes DC, Zayed AM, Ascenzi R, McCaskill AJ, Hoffman NE, Davis KR, Görlach J. 2001. Growth stage–based phenotypic analysis of Arabidopsis: a model for high throughput functional genomics in plants. *Plant Cell* **13**:1499–1510. doi:10.1105/TPC.010011

Chen VB, Arendall WB, Headd JJ, Keedy DA, Immormino RM, Kapral GJ, Murray LW, Richardson JS, Richardson DC. 2010. *MolProbity*: all-atom structure validation for macromolecular crystallography. *Acta Crystallogr, Sect D: Struct Biol* **66**:12–21. doi:10.1107/S0907444909042073

Christensen JB, Soares da Costa TP, Faou P, Pearce FG, Panjikar S, Perugini MA. 2016. Structure and Function of Cyanobacterial DHDPS and DHDPR. *Sci Rep* **6**. doi:10.1038/srep37111

Corral MG, Leroux J, Stubbs KA, Mylne JS. 2017. Herbicidal properties of antimalarial drugs. *Sci Rep* **7**. doi:10.1038/srep45871

Craciun A, Jacobs M, Vauterin M. 2000. *Arabidopsis* loss-of-function mutant in the lysine pathway points out complex regulation mechanisms. *FEBS Lett* **487**:234–238. doi:10.1016/S0014-5793(00)02303-6

Duke SO. 2012. Why have no new herbicide modes of action appeared in recent years? *Pest Manage Sci* **68**:505–512. doi:10.1002/ps.2333

Emsley P, Lohkamp B, Scott WG, Cowtan K. 2010. Features and development of *Coot*. *Acta Crystallogr, Sect D: Struct Biol* **66**:486–501. doi:10.1107/S0907444910007493

553 Evans PR, Murshudov GN. 2013. How good are my data and what is the resolution? *Acta*
554 *Crystallogr, Sect D: Struct Biol* **69**:1204–1214. doi:10.1107/S0907444913000061
555 Galili G, Amir R. 2013. Fortifying plants with the essential amino acids lysine and methionine
556 to improve nutritional quality. *Plant Biotechnol J* **11**:211–222. doi:10.1111/pbi.12025
557 Geng F, Chen Z, Zheng P, Sun J, Zeng A-P. 2013. Exploring the allosteric mechanism of
558 dihydrodipicolinate synthase by reverse engineering of the allosteric inhibitor binding
559 sites and its application for lysine production. *Appl Microbiol Biotechnol* **97**:1963–
560 1971. doi:10.1007/s00253-012-4062-8
561 Ghislain M, Frankard V, Jacobs M. 1995. A dinucleotide mutation in dihydrodipicolinate
562 synthase of *Nicotiana sylvestris* leads to lysine overproduction. *Plant J* **8**:733–743.
563 doi:10.1046/j.1365-313X.1995.08050733.x
564 Griffin MDW, Billakanti JM, Wason A, Keller S, Mertens HDT, Atkinson SC, Dobson RCJ,
565 Perugini MA, Gerrard JA, Pearce FG. 2012. Characterisation of the first enzymes
566 committed to lysine biosynthesis in *Arabidopsis thaliana*. *PLoS ONE* **7**:e40318.
567 doi:10.1371/journal.pone.0040318
568 Hall C, Soares da Costa T. 2018. Lysine: biosynthesis, catabolism and roles. *WikiJournal of*
569 *Science* **1**:4. doi:10.15347/wjs/2018.004
570 Hall CJ, Lee M, Boarder MP, Mangion AM, Gendall AR, Panjikar S, Perugini MA, Soares da
571 Costa TP. 2021. Differential lysine-mediated allosteric regulation of plant
572 dihydrodipicolinate synthase isoforms. *FEBS J* febs.15766. doi:10.1111/febs.15766
573 Hall CJ, Mackie ER, Gendall AR, Perugini MA, Soares da Costa TP. 2020. Review: amino
574 acid biosynthesis as a target for herbicide development. *Pest Manage Sci*.
575 doi:10.1002/ps.5943
576 Hall T. 1999. BioEdit: a user-friendly biological sequence aligment editor and analysis
577 program for windows 95/98/NT. *Nucelic Acids Symp Ser* **41**:95–98.
578 Heap I. 2021. The international survey of herbicide resistant weeds.
579 http://www.weedscience.com
580 Heap I. 2014. Global perspective of herbicide-resistant weeds. *Pest Manage Sci* **70**:1306–1315.
581 doi:10.1002/ps.3696
582 Hildebrandt TM, Nunes Nesi A, Araújo WL, Braun H-P. 2015. Amino acid catabolism in
583 plants. *Mol Plant* **8**:1563–1579. doi:10.1016/j.molp.2015.09.005
584 Hudson AO, Bless C, Macedo P, Chatterjee SP, Singh BK, Gilvarg C, Leustek T. 2005.
585 Biosynthesis of lysine in plants: evidence for a variant of the known bacterial pathways.
586 *Biochim Biophys Acta, Gen Subj* **1721**:27–36. doi:10.1016/j.bbagen.2004.09.008

587 Hutton CA, Perugini MA, Gerrard JA. 2007. Inhibition of lysine biosynthesis: an evolving
588 antibiotic strategy. *Mol BioSyst* **3**:458. doi:10.1039/b705624a
589 Jones-Held S, Ambrozevicius LP, Campbell M, Drumheller B, Harrington E, Leustek T. 2012.
590 Two *Arabidopsis thaliana* dihydrodipicolinate synthases, DHDPS1 and DHDPS2, are
591 unequally redundant. *Funct Plant Biol* **39**:1058–1067. doi:10.1071/FP12169
592 Kabsch W. 2010. *XDS*. *Acta Crystallogr, Sect D: Struct Biol* **66**:125–132.
593 doi:10.1107/S0907444909047337
594 Lindsey BE, Rivero L, Calhoun CS, Grotewold E, Brkljacic J. 2017. Standardized method for
595 high-throughput sterilization of Arabidopsis seeds. *JoVE* 56587. doi:10.3791/56587
596 Long F, Nicholls RA, Emsley P, Gražulis S, Merkys A, Vaitkus A, Murshudov GN. 2017.
597 *AceDRG*: a stereochemical description generator for ligands. *Acta Crystallogr, Sect D:*
598 *Struct Biol* **73**:112–122. doi:10.1107/S2059798317000067
599 McCoy AJ, Adams NE, Hudson AO, Gilvarg C, Leustek T, Maurelli AT. 2006. L,L-
600 diaminopimelate aminotransferase, a trans-kingdom enzyme shared by Chlamydia and
601 plants for synthesis of diaminopimelate/lysine. *Proc Natl Acad Sci USA* **103**:17909–
602 17914. doi:10.1073/pnas.0608643103
603 Murshudov GN, Skubák P, Lebedev AA, Pannu NS, Steiner RA, Nicholls RA, Winn MD,
604 Long F, Vagin AA. 2011. *REFMAC* 5 for the refinement of macromolecular crystal
605 structures. *Acta Crystallogr, Sect D: Struct Biol* **67**:355–367.
606 doi:10.1107/S0907444911001314
607 National Committee for Clinical Laboratory Standards. 2004. Standard for Antimicrobial
608 Susceptibility Testing, 13th Information Supplement. Wayne, Pa: NCCLS.
609 National Committee for Clinical Laboratory Standards. 2003. Methods for Dilution
610 Antimicrobial Susceptibility Tests for Bacteria that Grow Aerobically, Approved
611 Standard, 6th ed. Wayne, Pa: NCCLS.
612 Panjikar S, Parthasarathy V, Lamzin VS, Weiss MS, Tucker PA. 2005. *Auto-Rickshaw*: an
613 automated crystal structure determination platform as an efficient tool for the validation
614 of an X-ray diffraction experiment. *Acta Crystallogr, Sect D: Struct Biol* **61**:449–457.
615 doi:10.1107/S0907444905001307
616 Perl A, Galili S, Shaul O, Ben-Tzvi I, Galili G. 1993. Bacterial dihydrodipicolinate synthase
617 and desensitized aspartate kinase: two novel selectable markers for plant
618 transformation. *Nat Biotechnol* **11**:715–718. doi:10.1038/nbt0693-715
619 Perugini MA, Abbott B, Soares da Costa T. 2018. Heterocyclic inhibitors of lysine biosynthesis
620 via the diaminopimelate pathway. WO2018187845A1.

Peverelli MG, Perugini MA. 2015. An optimized coupled assay for quantifying diaminopimelate decarboxylase activity. *Biochimie* **115**:78–85. doi:10.1016/j.biochi.2015.05.004

Rasband WS. 2011. ImageJ, U.S. National Institutes of Health, Bethesda, Maryland, USA. *http://imagej.nih.gov/ij/*.

Sarrobert C, Thibaud M-C, Contard-David P, Gineste S, Bechtold N, Robaglia C, Nussaume L. 2000. Identification of an *Arabidopsis thaliana* mutant accumulating threonine resulting from mutation in a new dihydrodipicolinate synthase gene. *Plant J* **24**:357–368. doi:10.1046/j.1365-313x.2000.00884.x

Soares da Costa TP, Abbott BM, Gendall AR, Panjikar S, Perugini MA. 2017. Molecular evolution of an oligomeric biocatalyst functioning in lysine biosynthesis. *Biophys Rev* **10**:153–162. doi:10.1007/s12551-017-0350-y

Soares da Costa TP, Christensen JB, Desbois S, Gordon SE, Gupta R, Hogan CJ, Nelson TG, Downton MT, Gardhi CK, Abbott BM, Wagner J, Panjikar S, Perugini MA. 2015. Quaternary structure analyses of an essential oligomeric enzymeMethods in Enzymology. Elsevier. pp. 205–223. doi:10.1016/bs.mie.2015.06.020

Soares da Costa TP, Tieu W, Yap MY, Pendini NR, Polyak SW, Sejer Pedersen D, Morona R, Turnidge JD, Wallace JC, Wilce MCJ, Booker GW, Abell AD. 2012. Selective inhibition of biotin protein ligase from *Staphylococcus aureus*. *J Biol Chem* **287**:17823–17832. doi:10.1074/jbc.M112.356576

Soares da Costa TP, Desbois S, Dogovski C, Gorman MA, Ketaren NE, Paxman JJ, Siddiqui T, Zammit LM, Abbott BM, Robins-Browne RM, Parker MW, Jameson GB, Hall NE, Panjikar S, Perugini MA. 2016. Structural determinants defining the allosteric inhibition of an essential antibiotic target. *Structure* **24**:1282–1291. doi:10.1016/j.str.2016.05.019

Thompson JD, Higgins DG, Gibson TJ. 1994. CLUSTAL W: improving the sensitivity of progressive multiple sequence alignment through sequence weighting, position-specific gap penalties and weight matrix choice. *Nucl Acids Res* **22**:4673–4680. doi:10.1093/nar/22.22.4673

Tomé D, Bos C. 2007. Lysine requirement through the human life cycle. *J Nutr* **137**:1642S-1645S.

Tukey JW. 1977. Exploratory data analysis, Addison-Wesley series in behavioral science. Reading, Mass: Addison-Wesley Pub. Co.

654 Vats S. 2015. Herbicides: History, Classification and Genetic Manipulation of Plants for
655 Herbicide Resistance In: Lichtfouse E, editor. Sustainable Agriculture Reviews. Cham:
656 Springer International Publishing. pp. 153–192. doi:10.1007/978-3-319-09132-7_3
657 Vauterin M, Jacobs M. 1994. Isolation of a poplar and an *Arabidopsis thaliana*
658 dihydrodipicolinate synthase cDNA clone. *Plant Mol Biol* **25**:545–550.
659 doi:10.1007/BF00043882
660 Wang G, Xu M, Wang W, Galili G. 2017. Fortifying horticultural crops with essential amino
661 acids: a review. *Int J Mol Sci* **18**:1306. doi:10.3390/ijms18061306
662 Winn MD, Ballard CC, Cowtan KD, Dodson EJ, Emsley P, Evans PR, Keegan RM, Krissinel
663 EB, Leslie AGW, McCoy A, McNicholas SJ, Murshudov GN, Pannu NS, Potterton EA,
664 Powell HR, Read RJ, Vagin A, Wilson KS. 2011. Overview of the *CCP*4 suite and
665 current developments. *Acta Crystallogr, Sect D: Struct Biol* **67**:235–242.
666 doi:10.1107/S0907444910045749
667 Yugari Y, Gilvarg C. 1965. The condensation step in diaminopimelate synthesis. *J Biol Chem*
668 **240**:4710–4716.
669

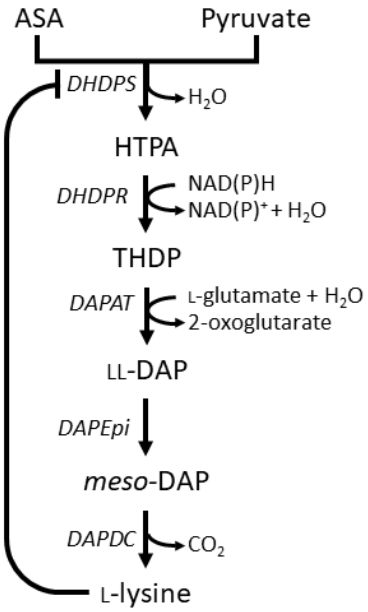
ASA
Pyruvate
DHDPS
H2O
HTPA
DHDPR
NAD(P)H
NAD(P)+ + H2O
THDP
DAPAT
L-glutamate + H2O
2-oxoglutarate
LL-DAP
DAPEpi
meso-DAP
DAPDC
CO2
L-lysine

A

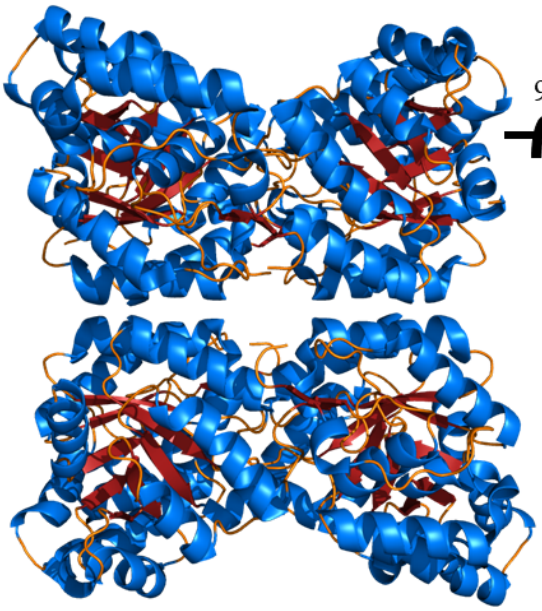

90°

B

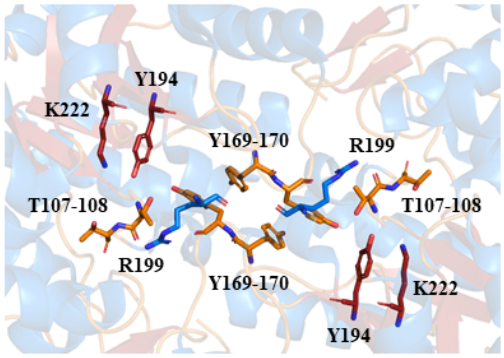

C

	107	169	194	199	222
At1	T	Y	Y	R	K
At2	T	Y	Y	R	K
Al1	T	Y	Y	R	K
Os1	T	Y	Y	R	K
Ta1	T	Y	Y	R	K
Vv1	T	Y	Y	R	K
Zm1	T	Y	Y	R	K
Ec	T	Y	Y	R	K

D

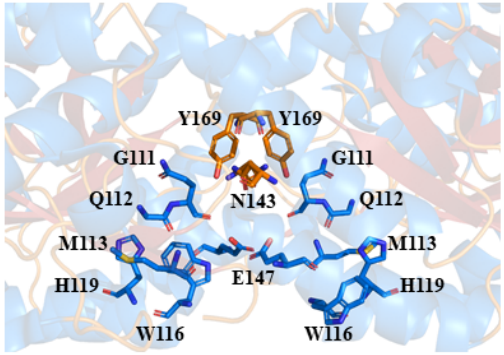

E

	111	119	143	147	169
At1	G	H	N	E	Y
At2	G	H	N	E	Y
Al1	G	H	N	E	Y
Os1	G	H	N	E	Y
Ta1	G	H	N	E	Y
Vv1	G	H	N	E	Y
Zm1	G	H	N	E	Y
Ec	S	H	N	E	Y

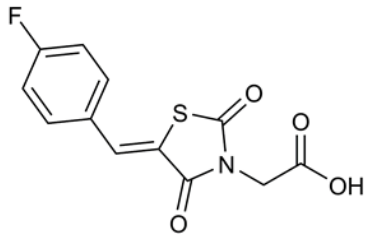

FBDTA

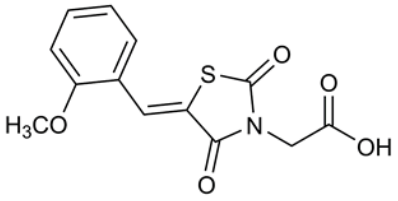

MBDTA-1

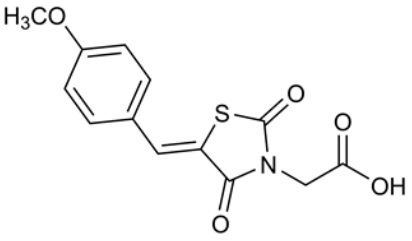

MBDTA-2

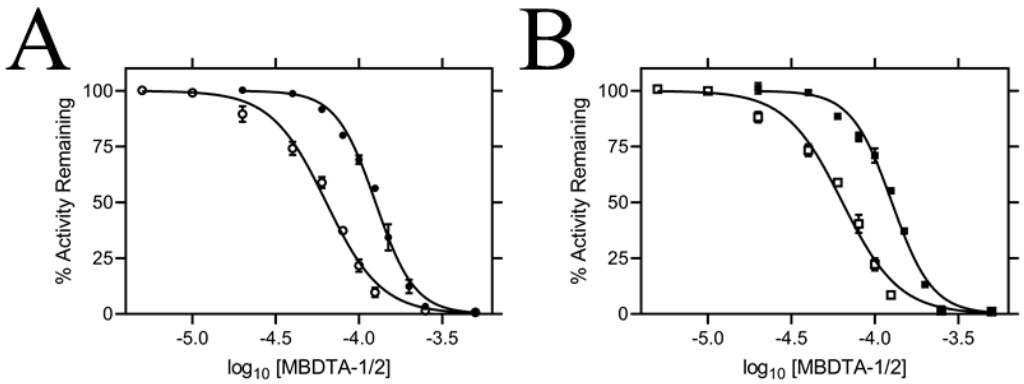
A
B
% Activity Remaining
100
75
50
25
0
-5.0
-4.5
-4.0
-3.5
log10 [MBDTA-1/2]

A

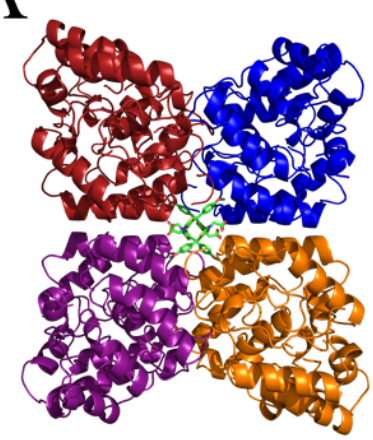

B

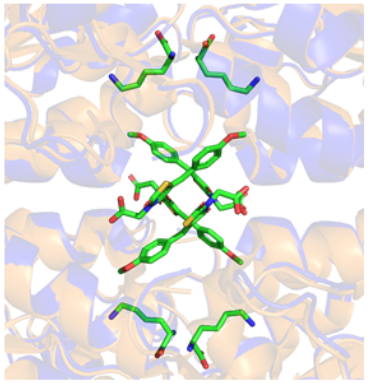

C

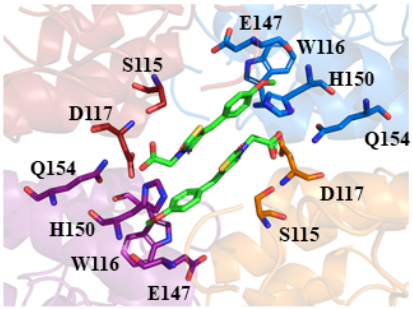

D

	115	147	150	154
At1	S	W	E	H	Q
At2	S	W	E	H	Q
Al1	S	W	E	H	Q
Os1	S	W	E	H	Q
Ta1	S	W	E	H	Q
Vv1	S	W	E	H	Q
Zm1	S	W	E	H	Q
Ec	N	H	E	S	R

A

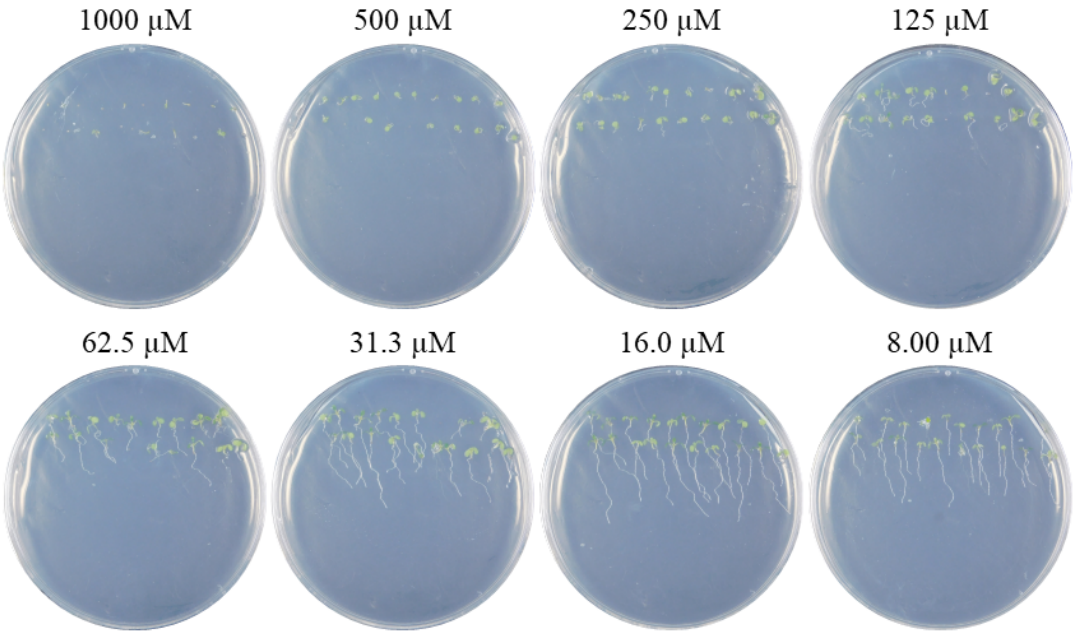
1000 µM
500 µM
250 µM
125 µM
62.5 µM
31.3 µM
16.0 µM
8.00 µM

B

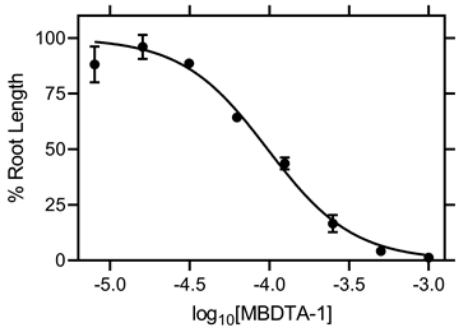
% Root Length
100
75
50
25
0
-5.0
-4.5
-4.0
-3.5
-3.0
log10[MBDTA-1]

A

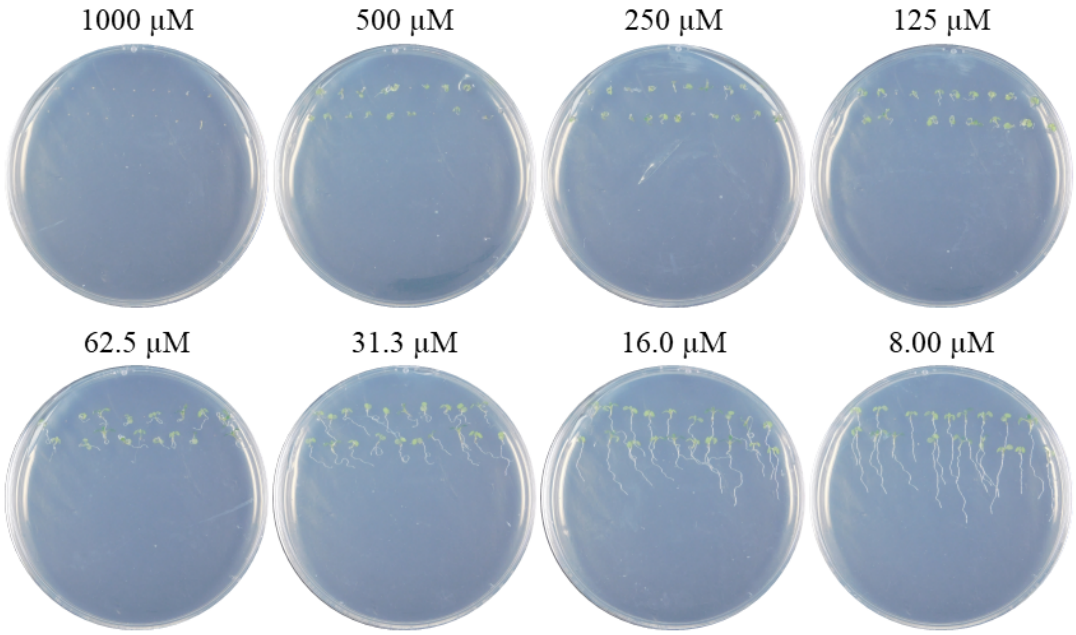
1000 µM
500 µM
250 µM
125 µM
62.5 µM
31.3 µM
16.0 µM
8.00 µM

B

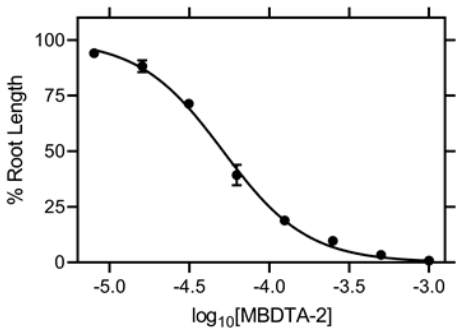
% Root Length
100
75
50
25
0
-5.0
-4.5
-4.0
-3.5
-3.0
log10[MBDTA-2]

A

B

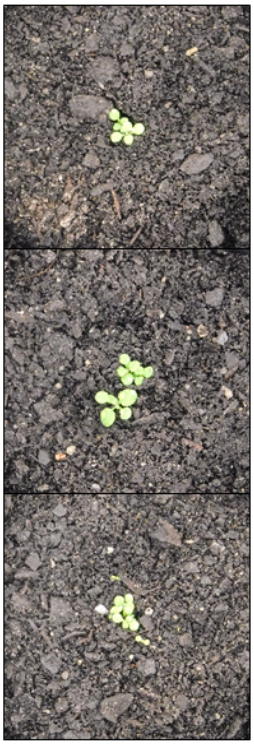

C

D

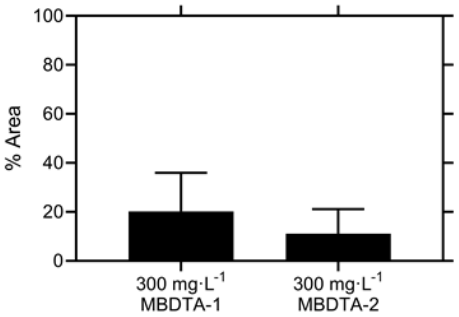

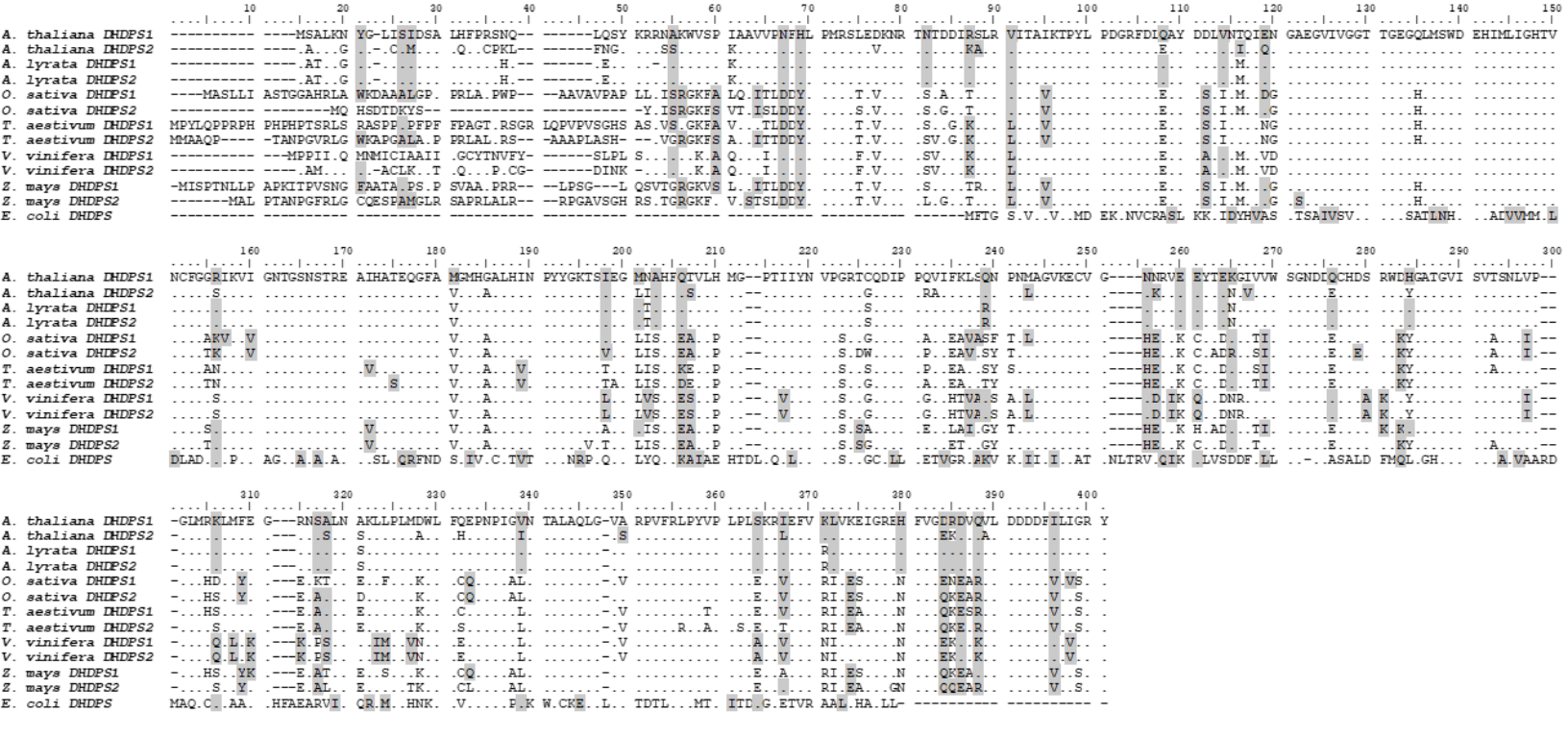
A. thaliana DHDPS1
A. thaliana DHDPS2
A. lyrata DHDPS1
A. lyrata DHDPS2
O. sativa DHDPS1
O. sativa DHDPS2
T. aestivum DHDPS1
T. aestivum DHDPS2
V. vinifera DHDPS1
V. vinifera DHDPS2
Z. mays DHDPS1
Z. mays DHDPS2
E. coli DHDPS

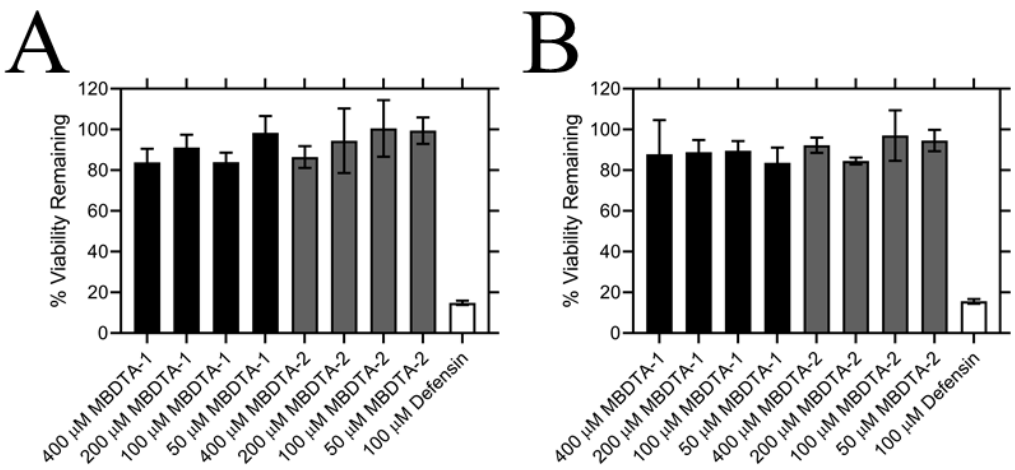
A
B
% Viability Remaining
120
100
80
60
40
20
0
400 μM MBDTA-1
200 μM MBDTA-1
100 μM MBDTA-1
50 μM MBDTA-1
400 μM MBDTA-2
200 μM MBDTA-2
100 μM MBDTA-2
50 μM MBDTA-2
100 μM Defensin